Chinese Herbal Medicines 11 (2019) 28–38

Contents lists available at ScienceDirect

Chinese Herbal Medicines

journal homepage: www.elsevier.com/locate/chmed

Original Article

Pharmacokinetic and NMR metabolomics approach to evaluate therapeutic effect of berberine and *Coptidis Rhizoma* for sepsis

Pei Li[a], Shan-ting Liao[a], Jun-song Wang[b,*], Qian Zhang[a], Yan Lv[a], Ming-hua Yang[a], Ling-yi Kong[a,*]

[a] *Jiangsu Key Laboratory of Bioactive Natural Product Research and State Key Laboratory of Natural Medicines, School of Traditional Chinese Pharmacy, China Pharmaceutical University, Nanjing 210009, China*
[b] *Center of Molecular Metabolism, Nanjing University of Science and Technology, Nanjing 210014, China*

ARTICLE INFO

Article history:
Received 15 April 2018
Revised 6 May 2018
Accepted 25 May 2018
Available online 16 October 2018

Keywords:
berberine
cecal ligation and puncture
Coptidis Rhizoma
metabolomics
sepsis

ABSTRACT

Objective: Sepsis, a systemic response to infection, often leads to end-organ dysfunction. Despite its high rates of mortality and morbidity, its pathophysiology is still poorly understood. *Coptidis Rhizoma* and its main active alkaloid compound, berberine, have been as anti-bacterial and anti-inflammatory drugs used in clinic. The objective of this study was to gain more insights towards understanding the sepsis associated with drug absorption and disposition and treatments of berberine and *Coptidis Rhizoma* dynamically.
Methods: Pharmacokinetic and metabolomic studies of *Coptidis Rhizoma* and its main active component berberine have been performed.
Results: Cecal ligation and puncture (CLP) induced sepsis showed marked changes of metabolites concerning energy metabolism and amino acids metabolisms, which could be reversed towards the normal state by *Coptidis Rhizoma* and berberine.
Conclusion: Berberine exhibited an equivalent and even better therapeutic effect than *Coptidis Rhizoma*.

1. Introduction

Sepsis, a systemic host response to infection, is characterized by a complex deregulation of inflammation resulting in multiple organ failure with high incidence and mortality (Wei et al., 2015). Despite rapid progress in medical care, sepsis treatment has been poorly progressed. Therefore, it is important to develop novel anti-sepsis drugs.

The CLP (cecal ligation and puncture) model is considered to be the gold standard in sepsis models (Rittirsch, Huber-Lang, Flierl, & Ward, 2009). CLP surgery, characterized by cecum ligation, damages the intestinal barrier, allowing bacterial translocation which ultimately leads to sepsis. The pathophysiological progress and comparable cytokine kinetics and magnitude after CLP surgery resembles with clinical sepsis.

Coptidis Rhizoma (Huanglian in Chinese, HL), a traditional herbal medicine, has been widely used for more than 2000 years. Numerous studies have shown that HL and its main active ingredients, coptis alkaloids have revealed therapeutic effects of anti-inflammatory and anti-oxidative (Meng et al., 2018; Tsai et al., 2016; Wu et al., 2018). As the major alkaloids of HL, berberine has been antibiotics and anti-inflammatory drug widely used in clinic. Modern biomedical studies on the pharmacological actions of berberine also demonstrated that berberine could attenuate the tissue injury and improve the survival rate in sepsis rats (Niu et al., 2011; Parisa & Hassan, 2018).

Pharmacokinetics (PK) is a study of the time course of absorption, distribution, metabolism and excretion (ADME) of a drug and how these processes vary between individuals. (Emilia, Paweł, Małgorzata, Roman, & Michał, 2017). In its general form, pharmacokinetic studies of HL and its main active component berberine have been performed to gain more insights towards understanding the phenomena associated with drug absorption and disposition (Peng et al., 2016).

Metabolomics is an analytical profiling technique for identifying and quantifying the variation of endogenous metabolites, which offers a window on metabolic mechanisms (Manchester & Anand, 2017). Because they intimately utilize and often rewire host metabolism, sepsis is an excellent choice to study by metabolomics techniques. Several analytical techniques have been used for metabolomics and metabolite profiling such as nuclear magnetic resonance (NMR) and mass spectrometry coupled with gas chromatography (GC–MS) (Barding, Beni, Fukao, Baileyserres, & Larive, 2013; Suarez-Diez et al., 2017). NMR is a popular analytical

* Corresponding authors.
E-mail addresses: wang.junsong@gmail.com (J.-s. Wang), cpu_lykong@126.com (L.-y. Kong).

https://doi.org/10.1016/j.chmed.2018.05.005
1674-6384/

platform for metabolite profiling, because it has advantages of relatively easy reference-free quantification, little sample preparation, nondestructive analysis nature, and universal detection for organic compounds (Mussap, Antonucci, Noto, & Fanos, 2013). Because of the inherent advantages of NMR, NMR platforms were used in this study to evaluate sepsis and treatments of berberine and HL dynamically.

In our previous studies, berberine and HL treatment effects were detected in septic mice induced by CLP. The aim of this study was to describe the pharmacokinetics and metabonomics of HL and berberine in CLP-induced septic rats dynamically.

2. Materials and methods

2.1. Chemicals and reagents

Berberine hydrochloride was purchased from Dalian Meilun Biotech Co., Ltd. (Dalian, China). Deuterium oxide (D_2O, 99.9%), sodium 3-trimethylsilyl-1-[2,2,3,3-$^2H_4$] propionate (TSP) were bought from Sigma Chemical Co. (St Louis, MO, USA). All reagents were of analytical grade.

2.2. Quantitative analysis by HPLC

Quantitative analysis was performed on an Agilent 1290 series equipped with an Agilent photodiode array detector (Agilent Technologies, Waldbronn, Germany). A standard solution for berberine was prepared in methanol. The amounts of berberine in HL extract were quantified. The mobile phase was composed of two parts: (A) 0.1% formic acid in water; (B) methanol, in a gradient program: 0–4 min, 10% B; 4–15 min, 10%–26% B; 15–27 min, 26%–28% B; 27–35 min, 28%–70% B; 35–55 min, 70%–90% B; 55–60 min, 90% B. The flow rate was set at 1 mL/min and the injection volume was 8 μL.

2.3. Animals and drug administration

Male 6-week-old Sprague–Dawley rats [(250 ± 20) g] were obtained from the Comparative Medicine Centre of Yangzhou University. Rats was housed in a well-ventilated and climate-controlled room at a relative humidity of (50 ± 10)% and a temperature of (25 ± 2) °C, with a 12 h light and dark cycle, with free access to water and rodent chow (5 rats per cage). All experiments were approved by the Animal Ethics Committee of the China Pharmaceutical University (AECCPU20160308), and conducted in accordance with the National Institutes of Health (NIH) guidelines for the Care and Use of Laboratory Animals.

After 7 d acclimatization, rats were randomly categorized into five groups ($n \geq 20$): CLP group (M), berberine + CLP group (Be), berberine + sham group (B), control group (S), *Coptidis Rhizoma* + CLP group (HL). Berberine and HL were in 0.5% solution of sodium carboxymethylcellulose. We modeled sepsis by subjecting the rats to the CLP procedure (Rittirsch et al., 2009). Briefly, rats were anesthetized with ketamine (100 mg/kg), then were dissected the midline of the abdomen. The cecum was ligated just below the ileocecal valve with 2-0 silk, the ligated cecal was then punctured twice with an 18-gauge needle, and a small amount of the intestinal contents was extruded through the puncture holes. After the bowel was returned to the abdomen, the incision was closed in two layers. At the end of the operation, all rats were resuscitated with saline (3 mL/100 g). Sham control rats were treated as described above except for cecal ligation and puncture. All animals were returned to their cages with free access and water, after 4 h, Be group: berberine (100 mg/kg) was ig administrated to CLP rats. B group: berberine (100 mg/kg) was ig administrated to sham rats. HL group: HL (378 mg/kg) was ig administrated to CLP rats. M group and S group were given water.

2.4. Sample collection

Blood specimens were obtained before dosing and subsequently at 5 min, 15 min, 30 min, 45 min, 1 h, 2 h, 3 h, 4 h, 6 h, 8 h, 12 h, and 24 h after drug administration. Then the plasma samples were obtained by centrifugation at 4°C, 3000 rpm for 10 min, and stored at −80°C. No obvious hemolysis was observed. A small volume (50 μL) of the plasma sample was added 400 μL acetonitrile solution included internal standard (IS) (2-isopropylmolic acid, 500 ng/mL), vortexed (5 min) and centrifuged (12 000 rpm, 10 min). The supernatant (400 μL) was evaporated to dryness. Then, the residue was reconstituted in 100 μL methanol-1% formic acid (10:90). After further centrifugation (12 000 rpm, 10 min), an aliquot of supernatant (5 μL) was injected into HPLC–MS/MS system for analysis.

A total of 300 mL 99.8% D_2O phosphate buffer (0.2 mol/L Na_2HPO_4 and 0.2 mol/L NaH_2PO_4, pH 7.0, containing 0.05% TSP) were added to 300 mL plasma samples at 4 h, 8 h, 12 h, and 24 h in order to minimize any NMR shift variation due to the pH discrepancy. After vortex and centrifugation to remove any debris, the supernatant (about 550 μL) was then pipetted into 5 mm NMR tube for ^{1}H-NMR analysis. TSP was used as the chemical shift reference, and D_2O provided the field frequency lock signal.

2.5. Pharmacokinetic study

2.5.1. Instrumental analysis

The analysis was performed as previously described (Liu, Wang, Yang, Jia, & Kong, 2013). Chromatography was performed on Agilent 1290 infinity system (Agilent Corp., Santa Clara, CA, USA). UPLC separations was done using Agilent Eclipse (100 mm × 2.1 mm, 1.7 μm) C_{18} column at 40°C. The mobile phase consisted of aqueous 0.1% formic acid solution (A) and acetonitrile with 0.1% formic acid (B). The optimal gradient conditions were as follows: 1%–20% B over 0–1 min, 20%–70% B over 1–3 min, 70%–85% B over 3–8 min, 85%–100% B over 8–9 min, the composition was held at 100% B for 1 min. The flow rate was 0.4 mL/min and injection volume was 1 μL. Detections of the separation were done by Agilent Q/TOF mass spectrometer (Agilent Corp., Santa Clara, CA, USA) equipped with an ESI interface. Optimized parameters were as follows: temperature 330°C; drying gas N_2 flow rate 10.0 L/min; nebulizer, 35 psig; fragmentor, 120 V; capillary voltage, 3500 V. The samples were analyzed in the positive ion mode in full scan (50–1000 Da) due to its sensitivity for the detection of berberine.

2.5.2. Method validation

The method was fully validated according to the Food and Drug Administration. The selectivity was evaluated by comparing blank plasma from eight different rats for interference. Calibration curve ($y = ax + b$) was analyzed by weighted ($1/X^2$) least squares linear regression. The lower limit of quantitation (LLOQ) was defined as the lowest concentration where the signal-to-noise (S/N) ratio was larger than 10 and both the precision (the relative standard deviation, RSD) and accuracy (relative error, RE) were less than or equal to 20% by analyzing the eight replicates of samples spiked with each analyze (Table 1). Linear regressions of the peak area ratios versus concentrations were fitted over the concentration range of 5–2000 ng/mL for berberine in rat plasma.

The intra-day accuracy and precision were determined within 1 d by analysis of eight replicates of QC samples at 4800 and 1600 ng/mL. The inter-day precision and accuracy were determined in three consecutive days. The accuracy and precision were depicted as relative error (RE) and RSD, respectively. The RE was within ± 15% and RSD did not exceed ± 15%. The intra-day and

inter-day and precision of the assay method for all analytes in rat plasma were shown in Table 2.

Recovery was evaluated by comparing the mean peak area of processed QC samples with the peak area of reference standards prepared in reconstitute solvent. The matrix effect was determined by comparing the peak areas of analytes in the above mentioned standard solutions with those of the neat standards at the same concentration. The stability of berberine in rat plasma was investigated by analysis of three levels of QC samples stored at −80 °C for two weeks (long-term stability), at 25 °C for 4 h (short-term stability) and after three freeze-thaw cycles (−80 °C–25 °C). Post-preparative storage was evaluated by analyzing the ready-to-inject samples placed in auto sampler at 4 °C for 24 h. The data for the absolute recovery and matrix effect were summarized in Table 3. All matrix effects were considered acceptable in this method. The data for short-term stability, long-term stability, freeze-thaw stability and post-preparative stability were shown in Table 4, also acceptable for routine analysis.

The developed and validated method was applied to determine berberine in rat plasma after administration. The mean concentration-time curves of berberine in plasma were shown in Fig. 1.

2.6. ^{1}H-NMR spectroscopy

All the spectra were recorded on a Bruker AV-500 MHz spectrometer (Bruker GmbH, Karlsruhe, Germany). To suppress the signals of proteins, a modified transverse relaxation-edited Call-Purcell-Meiboom-Gill (CPMG) sequence ($90(\tau\text{-}180\text{-}\tau)_n$-acquisition) was applied. Typically, 128 FIDs were collected into 32 K data points, spectral width of 10 000 Hz, an acquisition time per scan of 2.54 s, recycle delay of 2 s and a mixing time of 100 ms. Using TopSpin software (version 3.0, Bruker Biospin, Germany), all NMR spectra were manually phased, baseline corrected, and shift corrected to TSP at 0.00 parts per million.

The ^{1}H-NMR spectra were automatically exported to ASCII files using Mestre C (3.7.4, Mestrelab Research SL), then imported into "R" (http://cran.r-project.org/), and peak further aligned with an in-house developed R-script. The spectra were then binned into 0.015 parts per million integrated spectral buckets between 0.20

Table 1
Calibration curve, correlation coefficient (r^2), test range, weight cofficient and LLOQ for berberine in methanol solution ($n = 8$).

Sample	Compound	Calibration curve[a]	r^2	Liner range (ng•mL^{-1})	Weight cofficient	LLOQ[b] (ng•mL^{-1})
Plasma	Berberine	$Y = 0.023x - 0.00531$	0.9948	5–2000	$1/x^2$	5

[a] Y is peak area in LC-QTOF-MSMS for berberine; x is compound amount injected
[b] LLOQ refers to lower limits of quantitation.

Table 2
Precision and accuracy of berberine for QC samples in rat plasma ($n = 8$).

Sample	Compound	Concentration / (ng•mL^{-1})	RSD /%		Accuracy /%	
			Intra-day	Inter-day	Intra-day	Inter-day
Plasma	Berberine	4	6.48	5.64	−2.88	−2.28
		800	2.76	4.56	1.56	−3.48
		1600	5.52	6.24	−1.44	0.84

Table 3
Recovery and matrix effect for berberine in rat plasma ($n = 8$).

Sample	Compound	Nominal concentration/ (ng•mL^{-1})	Recovery (Mean ± SD, %)	RSD /%	Matrix effect (Mean ± SD, %)	RSD /%
Plasma	Berberine	4	89.4 ± 3.4	3.2	98.7 ± 4.2	4.6
		800	87.5 ± 7.3	5.1	92.2 ± 6.4	6.3
		1600	90.2 ± 4.5	4.4	98.1 ± 5.3	1.7

Table 4
Stability of berberine in plasma under various storage conditions ($n = 8$).

Compound	Condition	Concentration / (ng•mL^{-1})		RSD /%	Accuracy /%
		Added	Measured		
Berberine	Short-term stability	4	3.97 ± 0.10	2.76	−1.44
		800	789 ± 16	2.88	−1.08
		1600	1587 ± 115	6.96	−0.6
	Long-term stability	4	4.03 ± 0.07	1.08	0.84
		800	790 ± 20	1.44	−0.48
		1600	1590 ± 122	6.84	−0.72
	Freeze-thaw stability	4	3.88 ± 0.16	3.48	−2.28
		800	782 ± 14	2.4	−1.44
		1600	1578 ± 126	9.12	−1.2
	Post-preparative stability	4	3.85 ± 0.31	5.64	−3.96
		800	780 ± 18	3.24	−3.48
		1600	1573 ± 114	8.4	−0.48

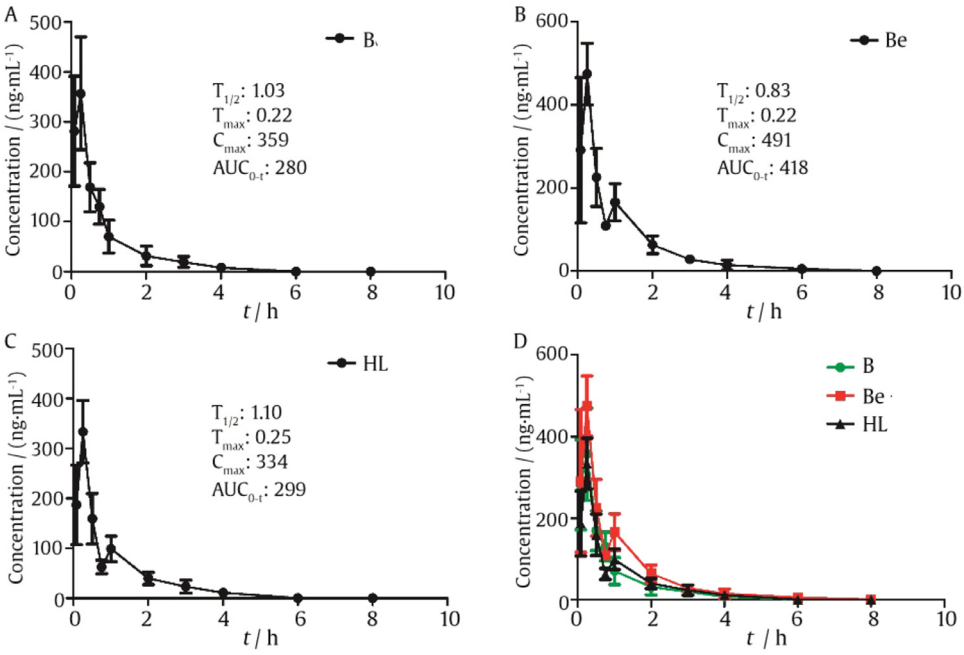

Fig. 1. Mean plasma concentration–time profiles of B (A), Be (B), HL (C), and overlay chart of three groups (D).

and 9.70. Regions of residual water resonances and its affected regions (4.70–9.70 parts per million) were removed to avoid their interference. The NMR data were binned, probabilistic quotient normalized, mean centered and pareto scaled before multivariate statistical analysis.

2.7. Data statistical analysis and peak assignments

Orthogonal partial least-squares discriminant analysis (OPLS-DA), a supervised multivariate statistical data analysis method, was executed by in-house developed scripts running in "R" software (http://cran.r-project.org/), used to remove unrelated variations through an orthogonal filter and identified the most significant variations among groups. The validity of the model was assessed by the parameters R^2 for the total explained variation and Q^2 for model predictability. The statistically significant metabolites in samples were evaluated by independent *t* test or Mann–Whitney test. The fold changes of metabolites and the associated *P*-values adjusted by BH (Benjamini-Hochberg) methods were calculated. $P < 0.05$ was considered statistically significant. Data were expressed in mean ± standard deviation (SD).

The signals were assigned by querying publicly accessible metabolomics databases, such as MMCD (http://mmcd.nmrfam.wisc.edu/), Madison (http://mmcd.nmrfam.wisc.edu/), HMDB (http://www.hmdb.ca/) and ECMDB (http:// www.ecmdb.ca/), aided by Chenomx NMR suite 7.5 (Chenomx Inc., Edmonton, Canada), and the statistical total correlation spectroscopy (STOCSY) analysis method (Holmes, Cloarec, & Nicholson, 2006; Kirwan, Coffey, Niere, Hawley, & Adams, 2009; Sonkar, Purusottam, & Sinha, 2012).

Metabolic pathway analysis (MetPA) was performed by Metaboanalyst (http:// www. metaboanalyst.ca) to reveal disturbed metabolism. Metabolic correlation networks were performed using the R-package igraph software.

Pearson correlation networks of metabolites were calculated using the "R" software. The networks could present the Pearson correlation coefficients among levels of metabolites and their structure similarity. In the networks, the nodes represent the metabolites, and the gray lines indicate that direct biological reactions exist between the connected nodes. Metabolites with correlation coefficients over 0.6 were joined with solid lines, colored in bluish to reddish corresponding to −1–1 of the correlation coefficients, whose widths were scaled according to their absolute values.

3. Results and discussion

3.1. Survival rate

Lipopolysaccharide (LPS) induced a high mortality (40.0%) of mice in CLP group, which could be totally avoided by HL treatment, and decreased by treatments of berberine to 13%.

3.2. Pharmacokinetic study

The PK profile for different groups showed that there were significant differences as shown in Table 5. The mean plasma concentration-time profiles of Be, HL, and B groups were depicted in Fig. 1. The validated method was successfully applied to determine the plasma concentrations of Be in rats following ig administration of Be and HL ($n = 8$ for each dose). The statistical analysis showed that there was no significant difference in T_{max} (time to reach maximum plasma concentration), $MRT_{0\text{-}t}$ (mean residence time), $MRT_{0\text{-}\infty}$. The statistical analysis has shown that there was significant difference in $t_{1/2}$, T_{max}, CL (clearance rate), $AUMC_{0\text{-}t}$ (areas under the first moment curves), $AUMC_{0\text{-}\infty}$, and Vd (volume of distribution) among the three groups ($P > 0.05$). The C_{max} (maximum plasma concentration) were respectively (490.67 ± 89.90) and (333.53 ± 62.46) ng/mL for the berberine and HL ($P = 0.0015$). This represents an increase of 1.47-fold. The mean half-life ($t_{1/2}$) was 0.83 h in Be group, obviously less than HL (1.10 ± 0.28), indicating that berberine was eliminated quickly than HL in rats. CL and $AUC_{0\text{-}\infty}$ were linearly related to the doses, showing that

Table 5
PK parameters of different groups.

Parameters	Units	B group	Be group	HL group	*P* value B *vs* Be group	*P* value Be *vs* HL group
$T_{1/2}$	h	1.03 ± 0.38	0.83 ± 0.24	1.10 ± 0.28	0.2487	0.0167
T_{max}	h	0.22 ± 0.07	0.22 ± 0.07	0.25 ± 0.00	1.0000	0.3632
C_{max}	ng•mL^{-1}	359.35 ± 110.95	490.67 ± 89.90	333.53 ± 62.46	0.0756	0.0015
AUC_{0-t}	h•ng•mL^{-1}	279.72 ± 46.91	417.51 ± 52.25	277.92 ± 60.75	0.0019	0.0001
$AUC_{0-\infty}$	h•ng•mL^{-1}	302.83 ± 43.06	443.15 ± 58.55	299.08 ± 65.11	0.0025	0.0001
Vz	mL•kg^{-1}	541127.75 ± 222646.99	297005.91 ± 90803.13	588754.73 ± 184633.02	0.0416	0.0013
Cl	mL•hr^{-1}•kg^{-1}	362167.26 ± 47121.84	246911.16 ± 29224.00	375159.98 ± 78338.63	0.0015	0.0025
$AUMC_{0-t}$	h•h•ng•mL^{-1}	237.45 ± 64.44	407.31 ± 48.26	281.46 ± 79.42	0.0006	0.0025
$AUMC_{0-\infty}$	h•h•ng•mL^{-1}	358.49 ± 132.42	539.54 ± 147.68	400.72 ± 136.85	0.0003	0.0180
MRT_{0-t}	h	0.86 ± 0.25	0.98 ± 0.09	1.01 ± 0.16	0.3067	0.6457
$MRT_{0-\infty}$	h	1.19 ± 0.43	1.22 ± 0.29	1.33 ± 0.31	0.8464	0.0964

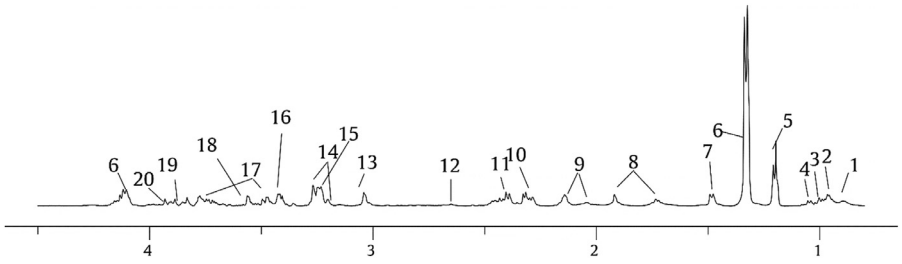

Fig 2. Typical 500 MHz ^{1}H NMR spectra of serum obtained from B, BE, HL, CLP, and sham groups. Metabolites in serum: 1. LDL/VLDL; 2. Isoleucine (Ile); 3. Leucine (Leu); 4. Valine (Val); 5. 3-hydroxybutyrate (3-HB); 6. Lactate (Lac); 7. Alanine (Ala); 8. Lysine (Lys); 9. Homoserine (Hom); 10. Pyruvate (Pyr); 11. Glutamate (Glu); 12. Citrate (Cit); 13. Creatine (Cr); 14. Cysteine (Cys); 15. Choline (Cho); 16. Taurine (Tau); 17. Glucose (Glc); 18. Glycine (Gly); 19. Phosphocreatine (PCr); 20. Threonine (Thr).

the pharmacokinetic process of berberine belongs to linear pharmacokinetics. Significantly highest area under the curve (AUC) values were observed in the Be group (417.51 ± 52.25 ng/h/mL) compared with HL group (277.92 ± 60.75 ng/h/mL) and B group (279.72 ± 46.91 ng/h/mL) with *P* values of 0.0001, 0.0019, respectively, indicating a 1.5-fold increase in the Be group, similar results were found in $AUC_{0-\infty}$. There was no significant difference in t_{max} among the three groups, (0.22 ± 0.07), (0.22 ± 0.07), (0.25 ± 0.00) for B, Be and HL groups, respectively. Significant differences were observed for apparent volume of distribution ($P = 0.0013$), and total body clearance ($P = 0.0025$) in Be and HL group. The time that drug's level below LLQQ was around 4 h. In order to describe holistic treatment effects, we produced metabonomics analysis at 4 h, 8 h, 12 h, and 24 h.

3.3. NMR metabonomics profile

3.3.1. Metabolites identification

Representative ^{1}H-NMR spectra for plasma samples were shown in Fig. 2. A total of 20 metabolites in the plasma were assigned.

3.3.2. OPLS-DA score of all groups at each time point

In the preliminary experiments, the binned NMR data were subjected to OPLS-DA analysis. In the OPLS-DA score plot (Fig. 3), the 12 mol/L group is the furthest apart from the sham group, among all the 4, 8, and 24 mol/L groups, which suggests that the most notable metabolic disturbance occurred 12 h after CLP model. To investigate the metabolic changes caused by CLP, an OPLS-DA

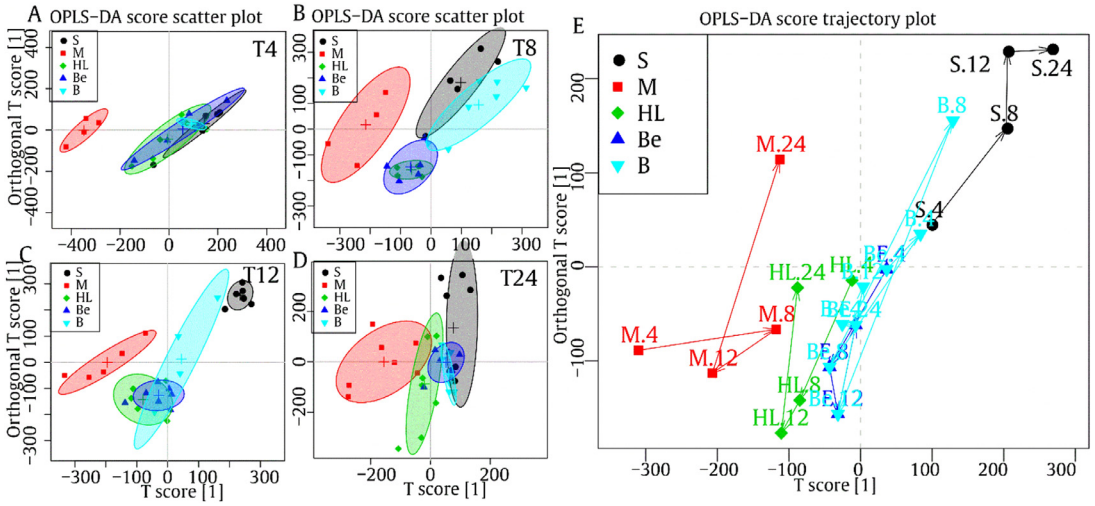

Fig. 3. OPLS-DA score trajectory plots of NMR data of different groups at 4, 8, 12, and 24 h after CLP model establishment.

model was established in the S and 12 M groups. The S, B, Be and HL group at four time points (4, 8, 12, and 24 h) showed separation from the M group, even overlapping with sham group, and then treatment groups was gradually close to the M group, which suggests that the best treatment effects after administration with drugs at 4 h. In addition, berberine has the equivalent treatment effects to HL.

3.3.3. Metabolomic analysis

To investigate the direct effect of CLP on rats, the OPLS-DA analysis was used to dynamically investigate the changed metabolites in plasma at four time points (4, 8, 12, and 24 h after CLP model). The ^{1}H NMR data from the normal control (NC) rats and the low dose VB-administered rats were evaluated at three time points (LT-2, LT-6, LT-12) using OPLS-DA analysis to dynamically investigate the time-dependent toxicity of VB at a dosage comparable to that used in clinic

The M and S groups were well separated OPLS-DA score plots (Fig. 4), indicating that the metabolic state of the rats was disturbed by CLP. The ^{1}H NMR data from the Be and M group were assessed by OPLS-DA analysis to dynamically investigate the treatment effects of berberine at four time points (4, 8, 12, 24 h after CLP model).The M and Be groups were well separated OPLS-DA score plots (Fig. 5), indicating berberine could relieve metabolic disorder induced by CLP, while the protect effects became weaken at 24 h.

Metabolites contributed to the differences between the groups were selected from the loading plots (Figs. 4 and 5) and Table 6 which was color-coded according to the absolute value of the correlation coefficient: a red signal indicated a more significant contribution to the class separation than a blue signal.

The metabolite line graph (Fig. 6) showed the changes and trends of M group, Be group, and S group. In general, compared with S rats, CLP model induced the disorder of metabolites:

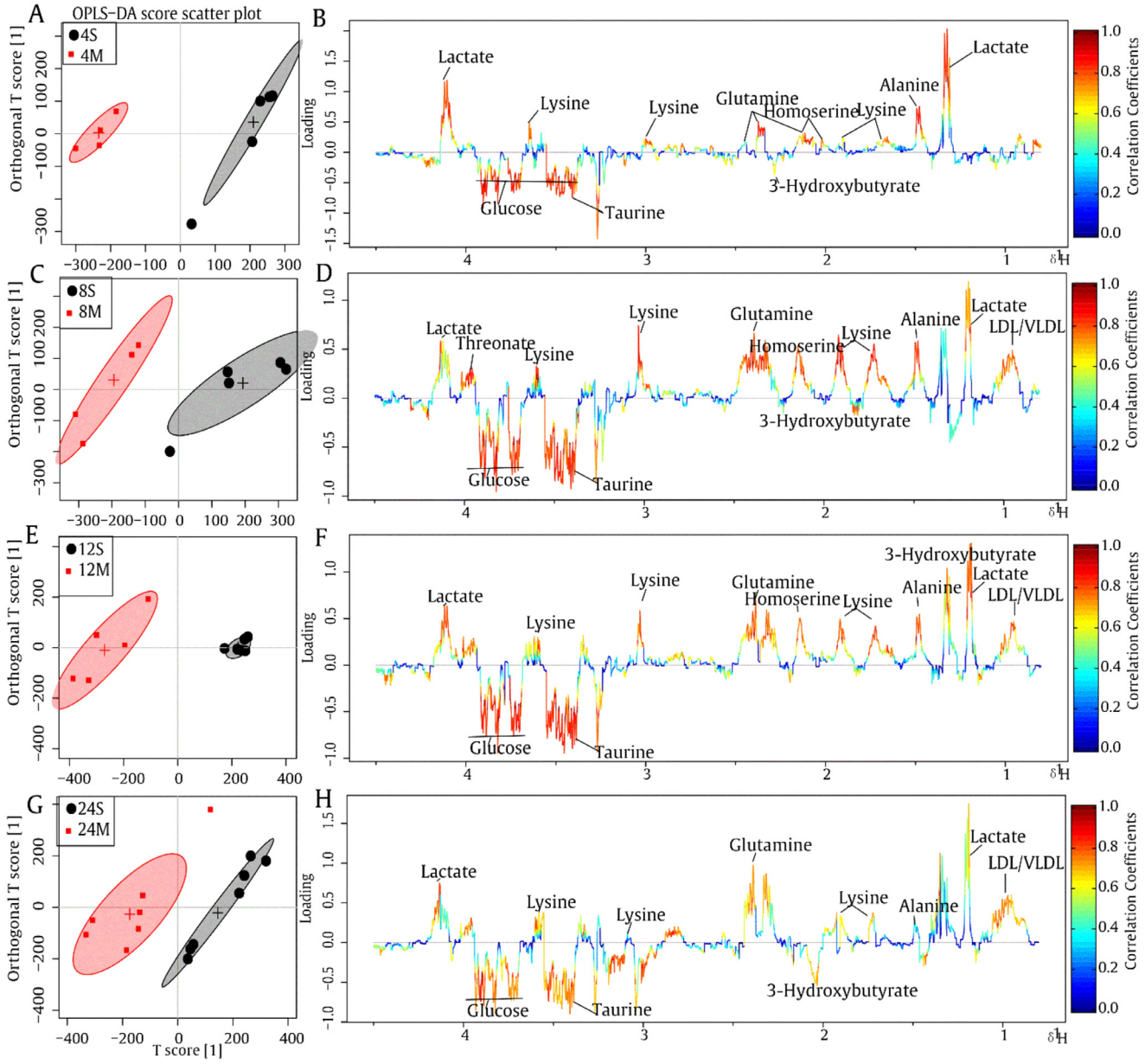

Fig. 4. Metabolomic profiles between S and M groups at 4, 8, 12, and 24 h. A, C, E, G: score plots for OPLS-DA; B, D, F, H: OPLS-DA loading plots color-coded according to absolute value of correlation coefficients.

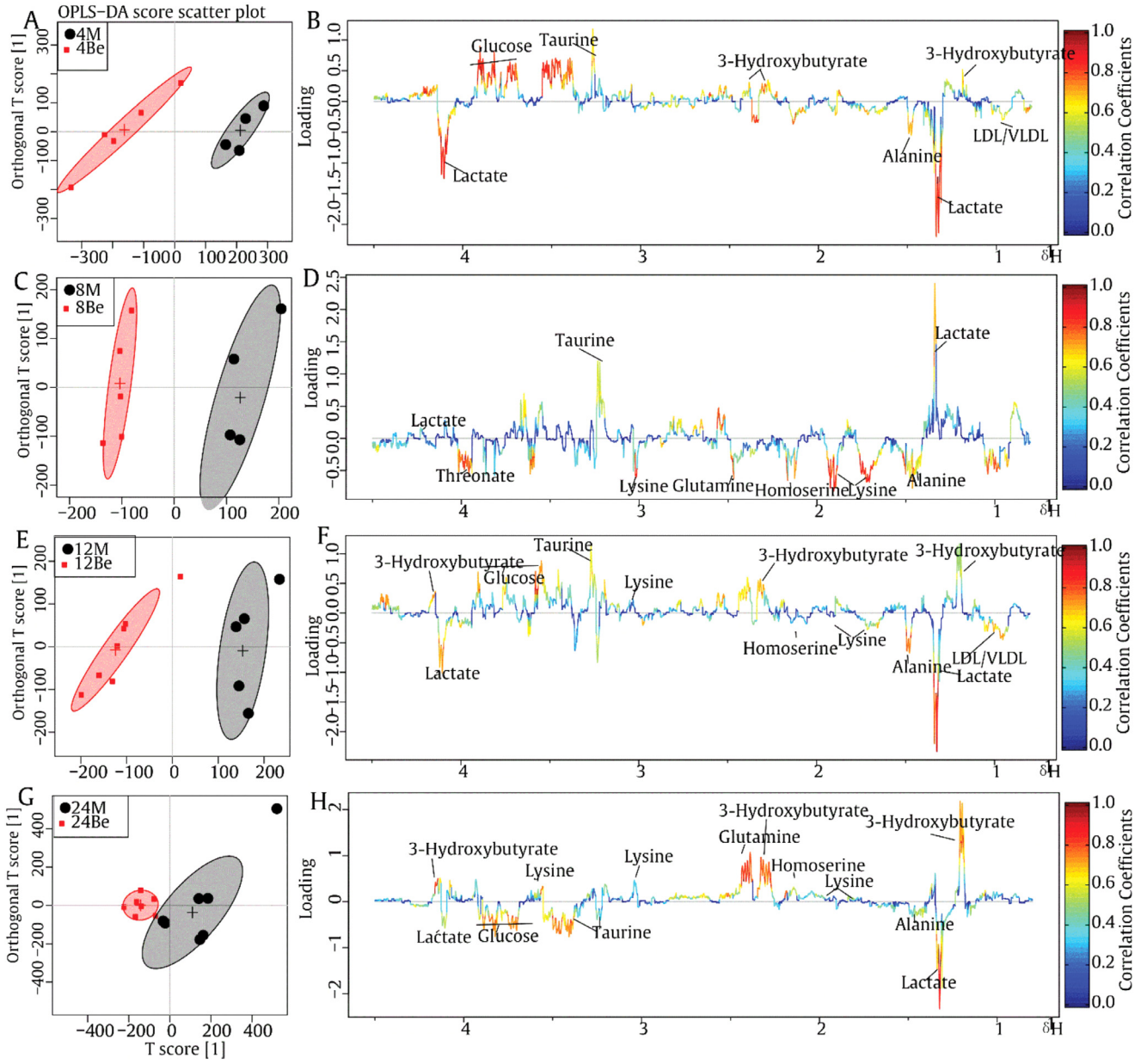

Fig. 5. Metabolomic profiles between M and Be groups at 4, 8, 12, and 24 h. A, C, E, G: score plots for OPLS-DA; B, D, F, H: OPLS-DA loading plots color-coded according to absolute value of correlation coefficients.

significantly increased levels of taurine, glucose, phosphocreatine (Pcr), glycine (Gly), obviously decreased levels of lactate (Lac), alanine (Ala), lysine (Lys), pyruvate (Pry), glutamate (Glu), isoleucine/leucine (Ile/Leu), Cr, Threonine (Thr), and those changes could be alleviated by berberine.

Pharmacodynamics evaluation combined with multivariate statistical analysis, univariate statistical analysis, and correlation network analysis (Fig. 7) revealed that CLP induced sepsis showed marked changes of metabolites concerning energy metabolism, amino acids metabolisms, oxidative stress as well as nucleic acid metabolism.

Compared with S group, significantly increased level of glucose, combined with obviously decreased levels of pyruvate, lactate and alanine was found in plasma of M group, indicating the blockage of glucose oxidation for energy supply and the disturbance in energy metabolism. Glucose was into pyruvate via glycolysis, (Alves, Alves, Costa, Castro, & Vinaud, 2017) producing adenosine triphosphate (ATP). Significantly increased level of glucose and obviously decreased level of pyruvate, suggested the hindered utilization of glucose, which caused accumulation of glucose and insufficient ATP generation. Lactate is the end-product of glycolysis (Harris et al., 2016; Love, Barrett & Hawkins , 2016), so its decease indicated an inhibited glycolysis.

The insufficient ATP supply results in an increasing reliance on of other means to produce energy, such as Creatine-Phosphocreatine (Cr-PCr) system and ketone bodies. The Cr-PCr system, through the creatine kinase (CK) reaction, (Hoerter, Ventura-Clapier, & Kuznetsov, 1994) plays crucial role in maintaining a constant ATP level. (Guzun et al., 2011; Kanazawa et al., 1998) The decreased Cr and increased PCr levels in the plasma suggested an accelerated conversion to ATP. Ketone bodies, e.g. 3-hydroxybutyrate (3-HB), may also serve as fuel if energy debt (Groscolas, 1986; Marat, Anton, Yuri, & Piotr, 2011). The ketone bodies were transferred from the plasma to organs to

Table 6
Identified metabolites from different groups with fold change and *P* value.

Metabolites	S *vs* M								M *vs* Be							
	4 h		8 h		12 h		24 h		4 h		8 h		12 h		24 h	
	Fold	*P*	Fold	*P*	Fold	*P*	Fold	*P*	Fold	*P*	Fold	*P*	Fold	*P*	Fold	*P*
LDL.VLDL	0.95		1.26		0.83		0.71	*	0.98		0.67		0.96		1.23	
Ile.Leu	1.05		0.79		0.78	***	0.71		1.00		1.16		1.08		0.92	
Val	1.16		0.90		0.91		0.86		0.96		1.27		1.15		0.78	
3.HB	1.05		0.52		0.49	*	0.61		0.97		0.79		0.84		0.82	
Lac	0.76	**	0.93		0.90	**	0.86		1.24	*	0.95		1.13	*	1.12	
Ala	0.53	***	0.75	*	0.71	**	0.83		1.31	*	1.15		1.26		1.24	
Lys	0.93		0.68	*	0.71	***	0.96		1.09		1.33		1.03		1.00	
Hom	0.82		0.80		0.68		1.40	**	1.23		1.09		1.18		0.89	
Pyr	0.62	**	0.64	*	0.68	**	0.84		1.21	*	1.12		0.89		0.88	
Glu	0.97		0.79		0.75	*	1.20		1.04		1.13		0.98		0.85	
Cit	1.06		0.96		1.02		1.31	*	0.80	*	0.82		0.84	*	0.72	*
Cr	0.97		0.90		0.89	*	1.14		1.06		0.93		0.84		0.84	
Cys	1.32	*	1.34		0.89		1.25		0.86		1.06		1.18		1.01	
Cho	0.96		1.06		1.03		1.54	*	1.03		0.81		0.84		0.75	
Tau	1.36	***	1.24	*	1.38	**	1.13		0.81	**	0.97		0.95		1.02	
Glc	1.46	**	1.58		2.05	***	1.87		0.76	*	1.02		0.92		1.08	
Gly	1.12	*	1.23		1.41	*	1.01		0.81	**	0.84		0.70		0.97	
PCr	1.38		1.23		1.13		1.54	*	0.78		0.98		0.93		0.75	
Thr	0.70		0.58		0.52	**	0.78		1.24		1.79		1.30		1.05	

*$P < 0.05$, **$P < 0.01$ and ***$P < 0.001$

replenish an insufficient energy supply, 3-HB was not significantly changed at 4 h, which was decreased along with time, suggesting its transfer from plasma to organs. The results indicated that energy metabolism was severely damaged in the M group. Berberine greatly improved the damaged energy metabolism in the M group as evidenced by their ability increase to energy availability. With the improved energy supply, the other energy production means were no longer necessary as exemplified by the decreased Cr and increased PCr levels, and reduced ketone body levels in Be group as compared with those in the M rats.

Significantly decreased level of glutamine was found in M group as compared with S group. Glutamine, serves as an essential metabolic precursor in nucleotide, energy metabolism, glutathione homeostasis, protein synthesis and so on. (Tapiero, Mathé, Couvreur, & Tew, 2002; Wu et al., 2015). Thus, the significantly decreased level of glutamine was found in M group showed its utilization during sepsis. Moreover, it has been shown that glutamine could reduce the extent of myocardial apoptotic cell death by decreasing the gene and protein expression of caspase-3 and be used to prevent the onset of sepsis at an early stage (Yin, Wei, Zhang, Ye, & Zhu, 2014). The markedly increased level of glutamine in Be group showed the ameliorative sepsis.

Taurine, the most abundant free amino acid (AA) in the body, influences cell function including regulation of cell osmotic and calcium homeostasis, anti-oxidant defense (Abdul & Dhanapal, 1997; Chang et al., 2004; Chou et al., 2015; Ghosh et al., 2008; Shimizu & Satsu, 2000); as a con-

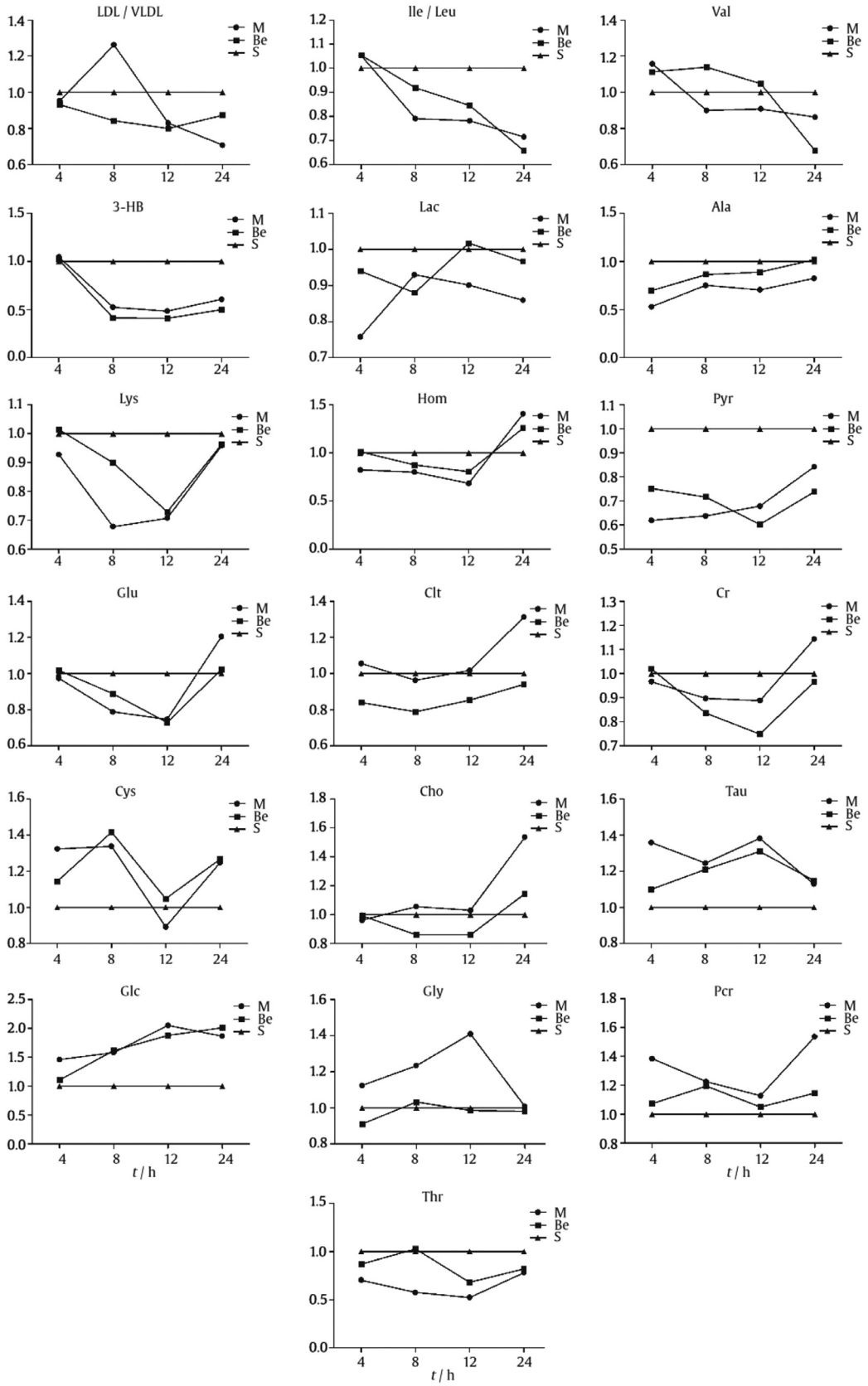

Fig. 6. Metabolite dynamic change line graph among S, M, and Be groups. S group was set as 1. Changes of M and Be groups at 4, 8, 12, and 24 h.

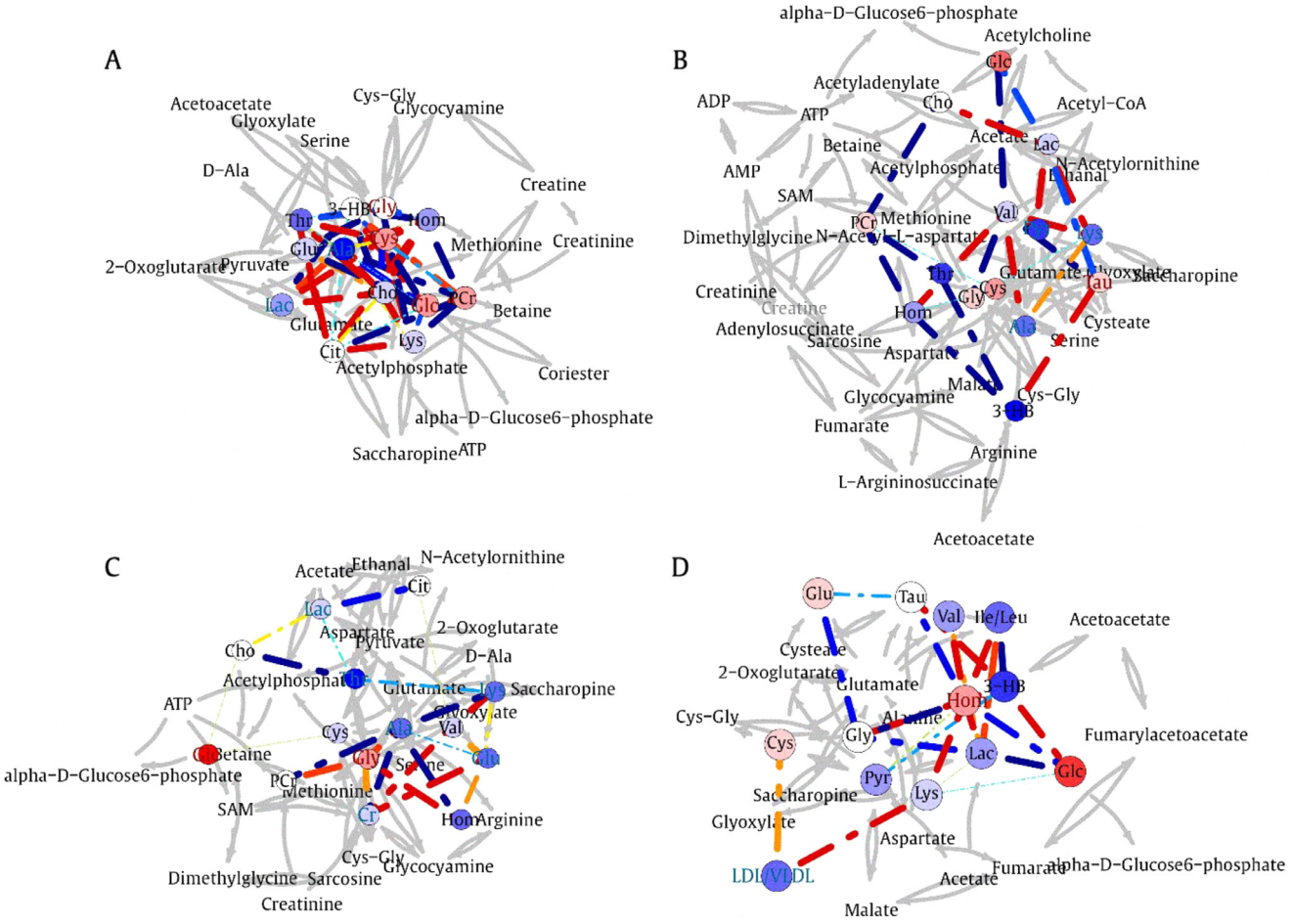

Fig. 7. Correlation network of differential metabolites between M and S group at T4 (A), T8 (B), T12 (C) and T24 (D) in serum. Only correlations with absolute values of correlation coefficients greater than 0.60 and P values < 0.05 were kept. Nodes represent metabolites, and lines between nodes indicated biological relationships between two corresponding metabolites. Red (blue) metabolites represented upregulated metabolites (downregulated metabolites) in M rats compared with sham rats or in drug-treated rats as compared with M rats. Solid lines between molecules indicated a correlation between molecules, line colors of red and blue displayed positive and negative relationships, respectively. Metabolites of similar structures were connected by dotted lines, indicating a possible biochemical reaction between molecules.

sequence, changes in taurine disposal have been associated with changes in immune competence and anti-inflammatory protection (Chiala, SiegeF, Boldrni, & Castagneto, 2000).

In our study, taurine was significantly increased in M group, which was supported by the previous research. It has been found experimentally that early increases in plasma taurine are elicited by the pro-inflammatory mediators of sepsis, are predictive of a more severe inflammatory response at pulmonary level, and that potentiation of taurine availability by exogenous support is protective against mediator-induced body dysfunction (Cantin, 1994; Viola, 2001).

Glycine was increased at highest level at 12 h, come back to normal at 24 h in M group as compared with S group. Glycine has gained attention due to its beneficial immunomodulatory effects in transplantation, shock and sepsis (Stoffels et al., 2011; Yang, Koo, Chaudry, & Wang, 2001; Zhong, Wheeler, Li, Froh, & Schemmer, 2003). Glycine reduces the immunoinflammatory response, the degree of distant organ injury, and the mortality rate, its increase in sepsis may be a self-protective mechanism. This great interest has been elicited by the evidence that requirement for glycine increases in sepsis for anti-oxidant and anti-inflammatory protection. It is normal in Be group which showed the mitigated metabolic disorders caused by CLP.

Significantly decreased levels of lysine and homoserine were found in M rats, which has been associated with systemic oxidative stress. The biosynthesis of homoserine and lysine begins with aspartic acid, a common intermediate in the biosynthesis of lysine and homoserine (Varisia et al., 2008; Viola et al., 2001). Homoserine dehydrogenase (HSD) is an oxidoreductase in the aspartic acid pathway (Navratna, Reddy, & Gopal, 2015). This enzyme coordinates a critical branch point of the metabolic pathway that leads to the synthesis of *L*-lysine, *L*-threonine, *L*-methionine, and *L*-isoleucine(Chen, Rappert, & Zeng, 2015). Body oxidative stress affected HSD expression, leading the synthesis disturbance of those amino acid. The AAAs (Isoleucine/Leucine, valine), and threonine increased up to 4 h, and then decreased follow time in M group, suggesting a synthesis disturbance counteracted the protein degradation follow times. Those phenomena were not obvious in Be group.

4. Conclusion

In summary, metabolomics analysis combined with correlation network analysis and pharmacokinetics revealed that CLP induced sepsis which showed marked changes of metabolites concerning energy metabolism and amino acids metabolisms, which could be reversed towards the normal state by berberine. Berberine exhibited an equivalent and even better therapeutic effect than HL. Combined pharmacokinetics and metabolomics approach dynami-

cally and holistically provided a promising tool for the study and better understanding of diseases and drugs.

Conflicts of interest

The authors declare that there is no conflict of interests regarding the publication of this paper.

Acknowledgments

This work was funded by the Key Project of the National Natural Science Foundation of China (No. 81430092, 81773857), the Program for Changjiang Scholars and Innovative Research Team in University (IRT_15R63), and the Priority Academic Program Development of Jiangsu Higher Education Institutions (PAPD).

References

Abdul, S. E., & Dhanapal, S. (1997). Effect of vitamin E and taurine treatment on lipid peroxidation and antioxidant defense in perchloroethylene-induced cytotoxicity in mice. *The Journal of Nutritional Biochemistry, 8*(5), 270–274.

Alves, D., Alves, L. M., Costa, T. L., Castro, A. M., & Vinaud, M. C. (2017). Anaerobic Metabolism in T4 Acanthamoeba Genotype. *Current Microbiology, 74*(6), 1–6.

Barding, G. A., Beni, J., Fukao, S., Baileyserres, J., & Larive, C. K. (2013). Comparison of GC–MS and NMR for metabolite profiling of rice subjected to submergence stress. *Journal of Proteome Research, 12*(2), 898–909.

Cantin, A. M. (1994). Taurine modulation of hypochlorous acid-induced lung epithelial cell injury *in vitro*. *Journal of Clinical Investigation, 93*(2), 606–614.

Chang, L., Zhao, J., Xu, J., Jiang, W., Tang, C. S., & Qi, Y. F. (2004). Effects of taurine and homocysteine on calcium homeostasis and hydrogen peroxide and superoxide anions in rat myocardial mitochondria. *Clinical and Experimental Pharmacology and Physiology, 31*(4), 237.

Chen, Z., Rappert, S., & Zeng, A. P. (2015). Rational design of allosteric regulation of homoserine dehydrogenase by a nonnatural inhibitor *L*-lysine. *ACS Synthetic Biology, 4*, 126–131.

Chiala, L. G., SiegeF, J. H., Boldrni, G., & Castagneto, M. (2000). Taurine and pulmonary hemodynamics in sepsis. *Amino Acids, 18*(4), 389–397.

Chou, C. T., Lin, H. T., Hwang, P. A., Wang, S. T., Hsieh, C. H., & Hwang, D. F. (2015). Taurine resumed neuronal differentiation in arsenite-treated N2a cells through reducing oxidative stress, endoplasmic reticulum stress, and mitochondrial dysfunction. *Amino Acids, 47*(4), 735–744.

Das, J., Ghosh, J., Manna, P., & Sil, P. C. (2008). Taurine provides antioxidant defense against NaF-induced cytotoxicity in murine hepatocytes. *Pathophysiology, 15*(3), 181–190.

Emilia, D. W., Paweł, W., Małgorzata, W. J., Roman, K., & Michał, J. M. (2017). Multilevel pharmacokinetics-driven modeling of metabolomics data. *Metabolomics, 13*(3), 31.

Groscolas, R. (1986). Changes in body mass, body temperature and plasma fuel levels during the natural breeding fast in male and female emperor penguins *Aptenodytes forsteri*. *Journal of Comparative Physiology. B, 156*(4), 521–527.

Guzun, R., Timohhina, N., Tepp, K., Gonzalez-Granillo, M., Shevchuk, I., Chekulayev, V., et al. (2011). Systems bioenergetics of creatine kinase networks: Physiological roles of creatine and phosphocreatine in regulation of cardiac cell function. *Amino Acids, 40*(5), 1333.

Harris, R. A., Tindale, L., Lone, A., Singh, O., Macauley, S. L., Stanley, M., et al. (2016). Aerobic glycolysis in the frontal cortex correlates with memory performance in wild-type mice but not the APP/PS1 mouse model of cerebral amyloidosis. *Journal of Neuroscience, 12*(7), 1871–1878.

Hoerter, J. A., Ventura-Clapier, R., & Kuznetsov, A. (1994). Compartmentation of creatine kinases during perinatal development of mammalian heart. *Molecular and Cellular Biochemistry, 133-134*(1), 277–286.

Holmes, E., Cloarec, O., & Nicholson, J. K. (2006). Probing latent biomarker signatures and *in vivo* pathway activity in experimental disease states via statistical total correlation spectroscopy (STOCSY) of biofluids: Application to $HgCl_2$ toxicity. *Journal of Proteome Research, 5*(6), 1313–1320.

Kanazawa, A., Tanaka, A., Iwata, S., Satoh, S., Hatano, E., Shinohara, H., et al. (1998). The beneficial effect of phosphocreatine Accumulation in the creatine kinase transgenic mouse liver in endotoxin-induced hepatic cell death. *Journal of Surgical Research, 80*(2), 229.

Kirwan, G. M., Coffey, V. G., Niere, J. O., Hawley, J. A., & Adams, M. J. (2009). Spectroscopic correlation analysis of NMR-based metabonomics in exercise science. *Analytica Chimica Acta, 652*(1-2), 173–179.

Liu, Q., Wang, J., Yang, L., Jia, Y., & Kong, L. (2013). A rapid and sensitive LC-MS/MS assay for the determination of berbamine in rat plasma with application to preclinical pharmacokinetic study. *Journal of Chromatogr B Analytical Technologies in the Biomedical and Life Sciences, 929*, 70–75.

Love, D., Barrett, T., & Hawkins, C. (2016). Hypothiocyanous acid (HOSCN) re-directs macrophage glycolytic flux through the pentose phosphate pathway-An adaption to oxidative stress in inflammation. *Free Radical Biology and Medicine*, S57.

Manchester, M., & Anand, A. (2017). Metabolomics: Strategies to define the role of metabolism in virus infection and pathogenesis. *Advances in Virus Research, 98*, 57–81.

Marat, M., Anton, L., Yuri, Z., & Piotr, B. (2011). Inhibition of spontaneous network activity in neonatal hippocampal slices by energy substrates is not correlated with intracellular acidification. *Journal of Neurochemistry, 116*(2), 316–321.

Meng, F. C., Wu, Z. F., Yin, Z. Q., Lin, L. G., Wang, R., & Zhang, Q. W. (2018). *Coptidis Rhizoma* and its main bioactive components: Recent advances in chemical investigation, quality evaluation and pharmacological activity. *Chinese Medicine, 13*(1), 13.

Mussap, M., Antonucci, R., Noto, A., & Fanos, V. (2013). The role of metabolomics in neonatal and pediatric laboratory medicine. *Clinica Chimica Acta, 426*, 127–138.

Navratna, V., Reddy, G., & Gopal, B. (2015). Structural basis for the catalytic mechanism of homoserine dehydrogenase. *Acta Crystallographica, 71*(5), 1216–1225.

Niu, L., Qiao, W., Hu, Z., Li, N., Huang, Q., Gong, J., et al. (2011). Berberine attenuates lipopolysaccharide-induced impairments of intestinal glutamine transport and glutaminase activity in rat. *Fitoterapia, 82*(3), 323–330.

Parisa, H., & Hassan, R. (2018). Preventive use of berberine in inhibition of lead-induced renal injury in rats. *Environmental Science and Pollution Research, 25*(5), 4896–4903.

Peng, S. L., Liu, L. F., Zhu, H. X., Li, B., Zhang, Q. C., & Guo, L. W. (2016). Effect of formula compatibility on berberine pharmacokinetics in brain tissue of rats. *Chinese Traditional Herbal Drugs, 47*(16), 2877–2882.

Rittirsch, D., Huber-Lang, M. S., Flierl, M. A., & Ward, P. A. (2009). Immunodesign of experimental sepsis by cecal ligation and puncture. *Nature Protocols, 4*(1), 31.

Shimizu, M., & Satsu, H. (2000). Physiological significance of taurine and the taurine transporter in intestinal epithelial cells. *Amino Acid, 19*(4), 605–614.

Sonkar, K., Purusottam, R. N., & Sinha, N. (2012). Metabonomic study of host-phage interaction by nuclear magnetic resonance- and statistical total correlation spectroscopy-based analysis. *Analytical Chemistry, 84*(9), 4063–4070.

Stoffels, B., Türler, A., Schmidt, J., Nazir, A., Tsukamoto, T., Moore, B. A., et al. (2011). Anti-inflammatory role of glycine in reducing rodent postoperative inflammatory ileus. *Neurogastroenterology and Motility, 23*(1), 76.

Suarez-Diez, M., Adam, J., Adamski, J., Chasapi, S. A., Luchinat, C., Peters, A., et al. (2017). Plasma and serum metabolite association networks: Comparability within and between studies using NMR and MS profiling. *Journal of Proteome Research, 16*(7), 2547–2559.

Tapiero, H., Mathé, G., Couvreur, P., & Tew, K. D. (2002). Glutamine and glutamate. *Biomedicine & Pharmacotherapy, 56*, 446–457.

Tsai, D., Stewart, P., Goud, R., Gourley, S., Hewagama, S., Krishnaswamy, S., et al. (2016). Pharmacokinetics of piperacillin in critically Ill Australian Indigenous patients with severe sepsis. *Antimicrobial Agents and Chemotherapy*. AAC.01657-16.

Varisia, V. A., Camargosb, L. S., Aguiarb, L. F., Christofoletia, R. M., Medicic, L. O., & Azevedoa, R. A. (2008). Lysine biosynthesis and nitrogen metabolism in quinoa (*Chenopodium quinoa*): Study of enzymes and nitrogen-containing compounds. *Plant Physiology and Biochemistry, 46*(1), 11–18.

Viola, R. E. (2001). The central enzymes of the aspartate family of amino acid biosynthesis. *Accounts of Chemical Research, 34*(5), 339–349.

Wei, Y., Gao, N., Zhang, Z., Zu, X., Hu, Z., Zhang, W., et al. (2015). Metabolic changes at the early stage of sepsis induced by cecal ligation and puncture in rats and the interventional effects of Huang-Lian-Jie-Du-Tang. *Journal of Chromatography B, 1026*, 176–182.

Wu, T. J., Lu, J., Ni, H., Li, P., Jiang, Y., & Li, H. J. (2018). Construction of an optimized method for quality evaluation and species discrimination of *Coptidis Rhizoma* by ion-pair high performance liquid chromatography combined with response surface methodology. *Journal of Pharmaceutical and Biomedical Analysis, 153*, 152–157.

Wu, X., Xie, C., Zhang, Y., Fan, Z., Yin, Y., & Blachier, F. (2015). Glutamate–glutamine cycle and exchange in the placenta–fetus unit during late pregnancy. *Amino Acids, 47*(1), 45–53.

Yang, S., Koo, D. J., Chaudry, I. H., & Wang, P. (2001). Glycine attenuates hepatocellular depression during early sepsis and reduces sepsis-induced mortality. *Critical Care Medicine, 29*, 1201–1206.

Yin, H. Y., Wei, J. R., Zhang, R., Ye, X. L., & Zhu, Y. F. (2014). Effect of glutamine on Caspase-3 mRNA and protein expression in the myocardium of rats with sepsis. *The American Journal of the Medical Sciences, 348*(4), 315–318.

Zhong, Z., Wheeler, M. D., Li, X., Froh, M., Schemmer, P., et al. (2003). L-Glycine: A novel antiinflammatory, immunomodulatory, and cytoprotective agent. *Current Opinion in Clinical Nutrition and Metabolic Car, 6*(2), 229–240.